JCTC Journal of Chemical Theory and Computation

Article

pubs.acs.org/JCTC

Challenges in Computing Electron-Transfer Energies of DNA Repair Using Hybrid QM/MM Models

Abdul Rehaman Moughal Shahi and Tatiana Domratcheva*

Department of Biomolecular Mechanisms, Max Planck Institute for Medical Research, Jahnstrasse 29, 69120, Heidelberg, Germany

Supporting Information

ABSTRACT: The influence of the molecular environment on chemical activity is an important factor in biomolecular mechanisms. We studied the effects of ionic groups, that is, a protonated histidine side chain and deprotonated phosphates of DNA, on electron transfer in light-induced DNA repair. On the basis of the X-ray crystal structure, we prepared a hybrid QM/MM model of the macromolecular complex formed between the (6–4) photolyase enzyme and the DNA substrate containing the thymine–thymine (6–4) photoproduct. At the optimized geometries, we computed with the CASSCF and CASPT2 methods the excited states of the electron donor and electron acceptor complex, consisting of the reduced flavin and the (6–4) photoproduct. The donor–acceptor complex interacts with its environment comprised of the protein, the double-stranded DNA substrate with its counterions, and the solvating water molecules, which we modeled using the AMBER94 force field. The excited states of our interest include two locally excited (LE) states of the flavin chromophore and intermolecular electron-transfer (ET) states. We identify only minor changes of the LE excitation energies by interactions with the environment, but in drastic contrast to that, we found significant changes of the ET excitation energies. In the presence of the positively charged His365H$^+$, the ET excitation energies decrease, indicating facilitated electron transfer. In addition, the excitation energy of the second LE state, explaining the flavin's absorption at 380 nm, undergoes a 0.2 eV downshift. In contrast to the active-site protonation, reduced screening of the DNA phosphates increases the ET excitation energies but not the LE excitation energies. Accordingly, the electron affinities of the (6–4) photoproduct are significantly reduced, which should hinder electron transfer from the excited flavin. We also show that dynamic electron correlation accounted by the second order perturbation theory CASPT2 does not alter the energy trends obtained with the CASSCF method. Including the histidine side chain in the QM part enhances the effect of the histidine protonation on the ET energies. We also note that protonated His365H$^+$ can serve as an electron acceptor.

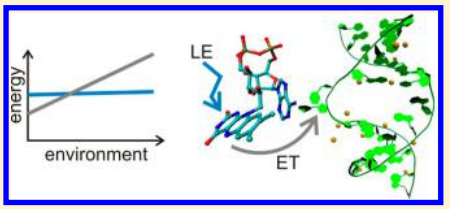

INTRODUCTION

Calculations of the excited electronic states of biomolecules using combined QM/MM approaches, involving application of high-level quantum-chemical methods coupled with the classical-mechanical description of the molecular environment, belong to the frontier of computational chemistry. Over the past several years, such computational studies accumulated evidence that ionic groups in biological cofactors, substrates, or enzymatic active sites play an important role in the excited state evolution. It is not seldom that the charged (protonated or deprotonated) side chains are found in the vicinity of the biological chromophores bound to their protein scaffolds. The well-known retinal and GFP chromophores undergo protonation inside the protein, which changes their UV–vis spectra and photodynamics implicated in the biological function. On the other hand, anionic groups such as phosphates are also very common in biomolecules. For instance, phosphodiester groups of DNA are deprotonated and thereby negatively charged at the physiological proton concentration. How this negative charge impacts chemical properties, in particular electron-acceptor properties implicated in the DNA photoinduced damage and repair, remains elusive.

In this study, we characterize a macromolecular complex between a double-stranded DNA molecule containing the (6–4) photoproduct of the two thymine bases and the DNA-repair enzyme, the (6–4) photolyase. The (6–4) photolyase is a light-dependent redox enzyme that specifically repairs the pyrimidine–pyrimidone (6–4) photoproduct using electron-donating properties of the flavin adenine dinucleotide (FAD) cofactor.[1−3] The DNA repair is triggered by light absorption of an antenna chromophore, folate, or deazaflavin, bound to the enzyme. Then, the excitation energy is transferred from the antenna to the reduced FADH$^-$ cofactor, which in turn donates an electron to the DNA photoproduct. The formed radical undergoes a repair reaction, which formally consists of formation of a covalent bond between the O4′H group and the 3′T base and cleavage of the covalent bond between the 5′T and 3′T nucleobases (Scheme 1). The repair is completed by return electron transfer from the repaired DNA to the FADH cofactor. In this complex process, redox potentials of the DNA photoproduct, repaired DNA, and flavin cofactor play a central role and should fall into a certain range to enable the complete electron transfer cycle. Whether this critical redox-potential balance is defined by the intrinsic properties of these

Received: June 25, 2013
Published: August 26, 2013

dx.doi.org/10.1021/ct400537b | J. Chem. Theory Comput. 2013, 9, 4644–4652

Scheme 1. The (6-4) Photoproduct and Two "Repaired" N1-Methyl-Thymine Molecules

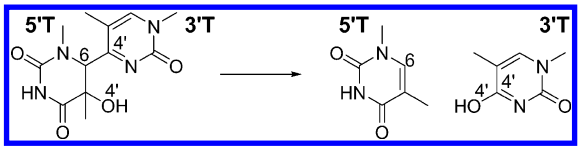

molecular entities or results from their interactions with the environment is still a subject of investigation.

Along with the electron transfer cycle, a proton transfer cycle from the conserved protonated residue His365H$^+$ to the (6−4) photoproduct and back has been proposed to take place.[6] Conserved His365 (in this study, we consider the *Drosophila melanogaster* enzyme) was suggested to be protonated even under alkaline conditions, at which the (6−4) photolyase shows higher repair activity *in vitro*.[4,5] According to the recently proposed repair scheme, His365H$^+$ protonates the (6−4) photoproduct after photoinduced electron transfer, which opens the repair channel.[6] Consistent with this hypothesis, only a futile electron transfer cycle was observed in a series of His365-mutated proteins.[6] On the other hand, contrary to the proposed "catalytic" DNA protonation, the efficiency of the enzymatic repair is reduced almost two times upon increasing the proton concentration from pH = 9 to pH = 7.[4] The protonation state of His365 under physiological conditions is unknown.

Determination of the (6−4) photolyase-DNA molecular structure by protein crystallography[7] stimulated computational investigations of the DNA repair mechanism.[8−15] Insight was acquired into electronic properties and chemical reactivity of the (6−4) photoproduct radical anion,[9] its repair reaction involving protonated histidine,[12,14] radical recombination via back-electron transfer,[14] ENDOR spectral signatures of the flavin radical,[13] electronic excitation energies,[9−11] and the protonation states of the repair active site.[11,13] At the same time, the role of the repair-site environment in tuning the redox potentials has not been studied so far. The repair molecular mechanism remains unresolved partly because of the uncertainty concerning the protonation state of the conserved His365. While some computational studies questioned the experimental assignment arguing that His365 is rather neutral,[11,13] the other studies, relying on the experimental assignments, proposed several DNA repair mechanisms involving protonated histidine.[12,14,15]

In our previous computational studies we considered the electron-acceptor properties of the (6−4) photoproduct.[9,11] We found that the (6−4) photoproduct consists of two electron-acceptor moieties—the pyrimidone 3′ base with the higher electron affinity and the pyrimidine 5′ base with the lower electron affinity.[11] Accordingly, the two ET states associated with these two electron acceptors have rather different excitation energies in the enzymatic repair site.[11] Proposed protonation of the 3′ base further significantly increases the electron affinity. Considering the (6−4) photoproduct of the two methyl-thymine bases (without the sugar phosphate backbone), we found that electron transfer coupled with the protonation of the photoproduct decreases the energy of the active site by more than 35 kcal/mol in the ground electronic state.[11] Such an electron transfer reaction in the electronic ground state (without photoexcitation) should deactivate the enzyme, which contradicts the current interpretation of the experimental observations. Whether this ground-state electron transfer is hindered in the macromolecular DNA-repair complex is still unknown. In the current study, we present hybrid QM/MM models of the repair complex to provide an answer to this question.

We study how interactions with the specific molecular environment influence the excitation energies of the repair site. We included the electron donor and the electron acceptor in the quantum-mechanical (QM) part, for which we carried out excited-state calculations with the multiconfigurational CASSCF-CASPT2 method. The interactions with the molecular mechanical (MM) part modeled with the AMBER94 force-field parameters are accounted with the electrostatic potential fitted (ESPF) operator.[16] We are interested in how the excitation energies of the repair site change depending on the protonation state of the conserved histidine, the distribution of the DNA counterions, and the presence of the water solvent. We also study the effects of dynamic electron correlation and the inclusion of the histidine side chain in the QM part.

MOLECULAR MODELS AND COMPUTATIONAL DETAILS

QM/MM Computational Scheme. We utilized the QM/MM electrostatic embedding approach with the ESPF operator[16] implemented on the basis of the MOLCAS[17,18] quantum-chemistry package and the Tinker[19] molecular-mechanics package. We carried out the state-averaged CASSCF[20] and the multistate (MS)CASPT2[21,22] calculations with the 6-31G* basis set.[23] To model the environment of the active site within the MM part, we used the AMBER94 force field[24] in combination with the TIP3P water parameters.[25]

Molecular Model of the Protein and DNA Complex. We prepared two QM/MM models containing either a protonated or neutral His365 side chain—the HisH$^+$ model and the His model, respectively. We used the coordinates of the crystal structure of the (6−4) photolyase from *Drosophila melanogaster* bound to a double-stranded DNA containing the T(6−4)T photoproduct of two thymines (PDB code 3CVU).[7] After inspecting the local environment, the following protonation states of the amino-acid side chains were assigned: His19, protonated (to satisfy a salt bridge with Glu224); all other His, the H−Nε form; all Glu and Asp, deprotonated; all Lys and Arg, protonated. The phosphates of the FADH$^-$ cofactor and of the DNA backbone were deprotonated. All crystal-structure water molecules were included in our models. The hydrogen atoms were added by using the Tinker program. To neutralize the overall electrostatic charge of the DNA−protein complex, 15 and 16 Na^+ counterions were added to the HisH$^+$ and His model, respectively, along the DNA backbone. A water shell of radius 50 Å consisting of 6000 water molecules was added using the package Packmol.[26] The coordinates of the water-shell molecules were optimized, keeping the coordinates of the protein and DNA constrained. After that, the energy minimization of the entire models was carried out keeping constrained the coordinates of the FADH$^-$ chromophore and the (6−4) photoproduct. The energy minimization was performed with the AMBER94 force field employing the Tinker program. The force field parameters and the atomic charges for the FADH$^-$ chromophore and the T(6−4)T photoproduct were taken from the previous studies.[27,28] The two obtained minimum-energy structures were used as starting structures in the QM/MM geometry optimization.

QM/MM Geometry Optimization. We performed QM/MM geometry optimization with the lumiflavin part (LFH$^-$) of

dx.doi.org/10.1021/ct400537b | J. Chem. Theory Comput. 2013, 9, 4644−4652

the $FADH^-$ cofactor and the T(6−4)T photoproduct (5′T base and 3′T base) in the QM part (62 atoms in total). The QM/MM boundary was accounted via hydrogen link atoms.[29] To avoid overpolarization of the QM part, the charges of the MM-boundary atoms were reassigned using the charge-shift scheme.[30] Three link atoms were introduced: one at the C1′−C2′ bond connecting lumiflavin to the ribityl chain and two at the two N1−C1′ bonds connecting the thymine bases to the deoxyribose moieties. The geometry optimization in the ground electronic state was performed using the CASSCF-(2,2)2 method. In the CASSCF(m,n)k notation, m and n indicate the number of electrons and molecular orbitals (MOs) in the active space, respectively, and k indicates the number of electronic states. In the CASSCF(2,2)2 calculations, the active space includes the highest occupied MO (HOMO) of flavin and the lowest unoccupied MO (LUMO) of the 3′ base. The geometry of the MM subsystem surrounding the QM part consisting of the amino acid residues His365, His369, Tyr423, Gln299, and Asn406; water molecule W697; the ribityl and adenine fragments of the $FADH^-$ cofactor; the two deoxyribose fragments; and the phosphate of the photoproduct was optimized at every QM-optimization step using the micro-iterations technique.[31] The coordinates of the other atoms of the MM part were constrained. In the geometry optimization course, the ESPF charges were computed with the state-averaged CASSCF electron density as implemented in MOLCAS version 7.6. The two energy-minimized structures so obtained, the $HisH^+$ model and the His model, were used for single-point energy calculations.

Modification of the MM Part. To study how the DNA negative charge influences the excitation energies, we considered several modifications of the MM part. In our QM/MM models, the double-stranded DNA contains 28 negatively charged phosphates included in the MM part. Their negative charge is screened by interactions with the protein, water molecules, and Na^+ counterions. In the initial protein−DNA model, we placed, depending on the protonation state of His365, 15 or 16 Na^+ counterions along the DNA sugar−phosphate backbone. We identify the counterions by their distances to the phosphorus atom in the phosphodiester group of the (6−4) photoproduct. Because of the similar initial structures, the distributions of the Na^+ ions in our $HisH^+$ and His QM/MM-optimized models are very similar. To decrease the screening of the DNA negative charge, we moved one or two ions from their position that is proximal to the repair site to a remote position of about 30 Å. We refer to the model with the modified MM part by indicating the displaced Na^+ ion(s), e.g., MM-2.7 or MM-(2.7 + 7.7). In the case of the $HisH^+$ model, we also quantify the effect of the water solvent by removing the entire water shell; this model is designated as MM-W. We did not reoptimize the geometry of the modified MM part; this simplified computational procedure satisfies our main goal to compare the change in the excitation energies of the LE and ET states with the different electronic structure.

Excitation Energies. We computed excitation energies of the repair active site using several approaches: by varying the content of the QM part, by introducing the described modifications of the MM part, and also by considering a different number of electronic states. The complete list of our models is given in the Supporting Information. First, we considered the (D,A) models that contain the electron donor and the electron acceptor in the QM part (like we did in the QM/MM geometry optimization). Then, we extended the QM part to (D,A,H) by including the histidine side chain. A hydrogen link-atom was incorporated in the Cα−Cβ bond of His365. The size of the QM part is increased to 79 and 78 atoms with $HisH^+$ and His, respectively. The histidine side-chain geometry was optimized using the force-field parameters and not quantum-mechanically. To compute the excitation energies of the (D,A) and (D,A,H) QM/MM models, the following CASSCF calculations were carried out. First, we consider only one excited state which corresponds to the ET of the 3′ base computed with the CASSCF(2,2)2 method. In the case of the $HisH^+$(D,A,H) model with the modified MM part MM-6.9 and MM-(2.7 + 7.7), the ET-3′T state was the second excited state, whereas the ET-$HisH^+$ state was the first excited state. For these two models, we computed the excitation energies with the CASSCF(2,3)3 method considering both excited states. Second, we computed five electronic states with the CASSCF(2,5)5 method considering the two lowest-energy LE states of flavin, the ET-3′T and ET-5′T states, and the closed-shell ground state. The five-state calculations are significantly more time-consuming than the two-state calculations; therefore we performed them only with the smaller (D,A) QM part. All CASSCF calculations were carried out using state-averaging with equal weights for all considered electronic states. The effect of dynamic electron correlation on the excitation energies was accounted for by using the multistate extension of the second-order multiconfigurational perturbation theory (MS)CASPT2 method. The standard IPEA shift[32] of 0.25 au and an imaginary shift[33] of 0.1 au were used.

Energy Decomposition. The total energy of the molecular system consists of the quantum-mechanically computed QM/MM energy and the MM energy that includes all classically defined terms. The MM energy is the same for all electronic states and, thus, does not influence the excitation energies. In the excitation energy analysis, we compare only the QM/MM energies. The QM/MM energy is the energy of the QM part that interacts, through the ESPF operator, with the surrounding electrostatic charges. We computed the QM/MM interaction energy by subtracting the QM/MM energy from the QM energy of the free QM part (no surrounding charges). The QM energy is computed at the same geometry as the QM/MM energy. The interaction energy has a positive sign and corresponds to the amount of energy by which the total QM energy is lowered by introducing the ESPF operator in the Hamiltonian. We compare the QM/MM interaction energy with the ESPF energy,[31] which is the energy of the electrostatic interactions of the MM-part RESP charges as defined by the AMBER94 force field and the QM-part ESPF charges fitted using the CASSCF electron density of each electronic state polarized by the embedding. The difference between the QM/MM interaction energy and the ESPF energy we consider as the polarization energy of the QM part by the MM part. We note that our definition of the polarization energy here is different from the one used in the original ESPF paper,[31] which considers the change of the ESPF interaction energy due to the QM-part polarization as the polarization energy.

RESULTS

Optimized Geometry of the Active Site. The active site of the DNA repair complex and the distribution of the Na^+ counterions with respect to the DNA backbone are shown in Figure 1. The optimized geometries of the flavin hydroquinone anion and (6−4) photoproduct in the $HisH^+$ and His models are very similar (the bond distances are compared in Figure S1

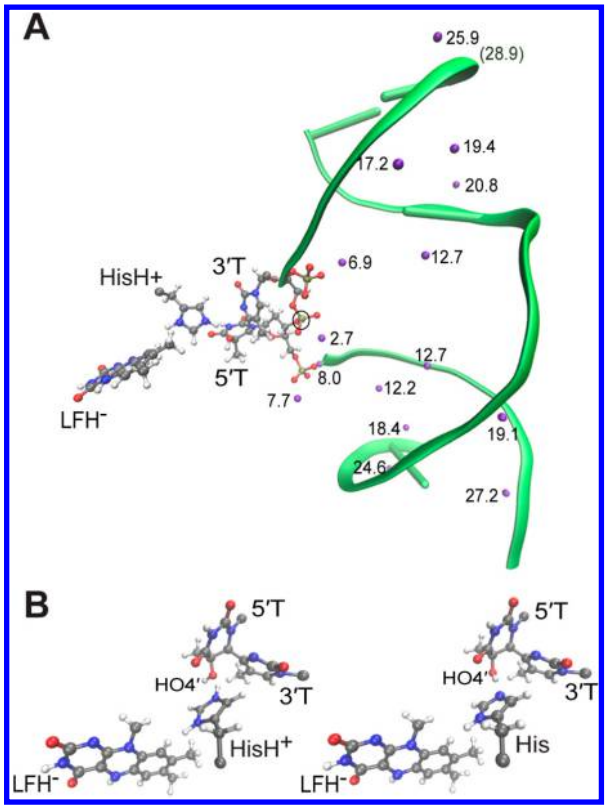

Figure 1. Structure of the DNA-repair site. (**A**) In the $HisH^+$ model, we indicate the electron-donor lumiflavin (LFH^-), (6–4) photoproduct (3′T and 5′T), histidine side chain ($HisH^+$), and the Na^+ counterions (by their distances form the phosphorus atom in the circle). (**B**) In the (D,A,H) QM part, we indicate the O4′H group of the photoproduct, which is transferred from 5′T to 3′T in the repair course.[9]

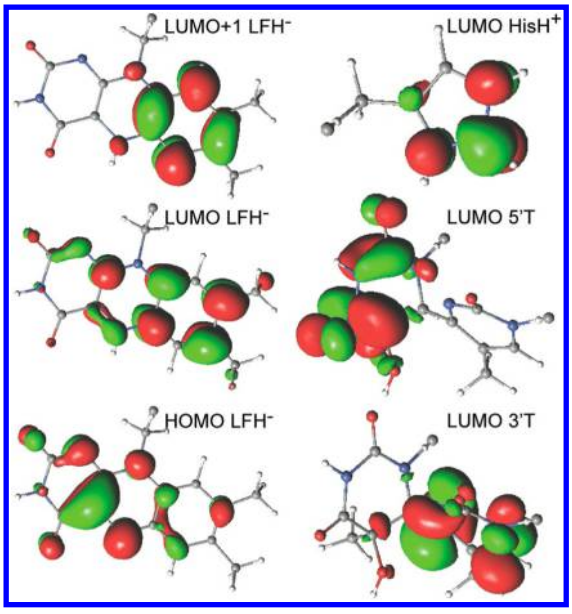

Figure 2. The CASSCF-optimized MOs of the complete active space.

in the Supporting Information). The major difference is found for the orientation of the O4′H group of the 5′ base that interacts with His365 either as a hydrogen-bond donor or a hydrogen-bond acceptor. The respective hydrogen-bond distance is equal to 2.7 Å in both models, which is equivalent to the distance in the parent crystal structure. The previous studies employing classical molecular-dynamic simulations[13] and geometry optimization of molecular clusters[11] indicated that the hydrogen bond formed by protonated $His365H^+$ has a longer $N\delta\cdots O4'$ distance than that of the neutral counterpart. Evidently, the constraints implicated in the QM/MM geometry optimization do not allow accounting for this difference.

Excitation Energies. All together, we computed six electronic states of the repair active site. The MOs of the complete active space are shown in Figure 2. The ground state has a closed-shell structure with the doubly occupied HOMO of flavin. In all excited states, the singly occupied HOMO of flavin is combined with one of the singly occupied LUMOs. The LE1 and LE2 states of flavin have singly occupied LUMO and LUMO+1 of flavin; the ET-3′T, ET-5′T, and ET-$HisH^+$ states have singly occupied LUMO of the 3′T base, LUMO of the 5′T base, and LUMO of the protonated $HisH^+$, respectively.

The computed excitation energies are presented in Figure 3. Unless otherwise stated, we discuss the results obtained with the (MS)CASPT2 method. Computations of the closed-shell ground state and the ET-3′T state with the CASSCF(2,2)2 method provide the simplest model of electron transfer in the photolyase–DNA complex. The ET-3′T excitation energy decreases if the histidine is protonated as presented in Figure 3A. The magnitude of the decrease is larger if the histidine side chain is included in the QM part. In the (D,A,H) QM models with protonated and neutral histidine, the excitation energies differ by 1.13 eV. Adding the MM part "compensates" the effect, and the energy difference decreases to 0.57 eV. If the histidine side chain is included in the MM part, the energy difference further reduces to 0.25 eV. The CASSCF method systematically overestimates the excitation energy by about 0.6 eV compared to the (MS)CASPT2 method. However, the parallel lines in Figure 3A and B demonstrate that the environmental effects do not differ to any appreciable extent with the CASSCF and CASPT2 methods, revealing that the effects of dynamic electron correlation and the environment are largely additive for the considered cases.

The excitation energies computed with the modified MM part, in which the negative charge of DNA is less screened, are presented in Figure 3B. A series of modifications was considered for the $HisH^+$(D,A) model, whereas for the other models only the limiting case of two ions removed, MM-(2.7 + 7.7) or MM-$2Na^+$, was computed. In the modified models, the ET excitation energies increase, which is consistent with the reduced electron affinity of the photoproduct. We computed the largest effect by removing two ions at distances of 2.7 and 7.7 Å. Removing the 2.7-Å ion increases the energy by 1.0 eV, whereas removing the 7.7-Å ion does so by 0.5 eV. Removing the two ions simultaneously increases the energy by 1.5 eV. The additive effect indicates the dominating role of electrostatic interactions. Ions located farther than 12 Å away from the active site cause only a small effect. Removing the entire water shell but keeping all counterions and the crystal-structure water molecules increases the energy by about 1 eV, which is equivalent to removing the closest counterion to the active site. From this result, it is obvious that solvating DNA in a QM/MM model is important for evaluation of the ET energies. There is a systematic difference in the excitation energies of the $HisH^+$ and His models independent of the MM-part modifications.

dx.doi.org/10.1021/ct400537b | J. Chem. Theory Comput. 2013, 9, 4644–4652

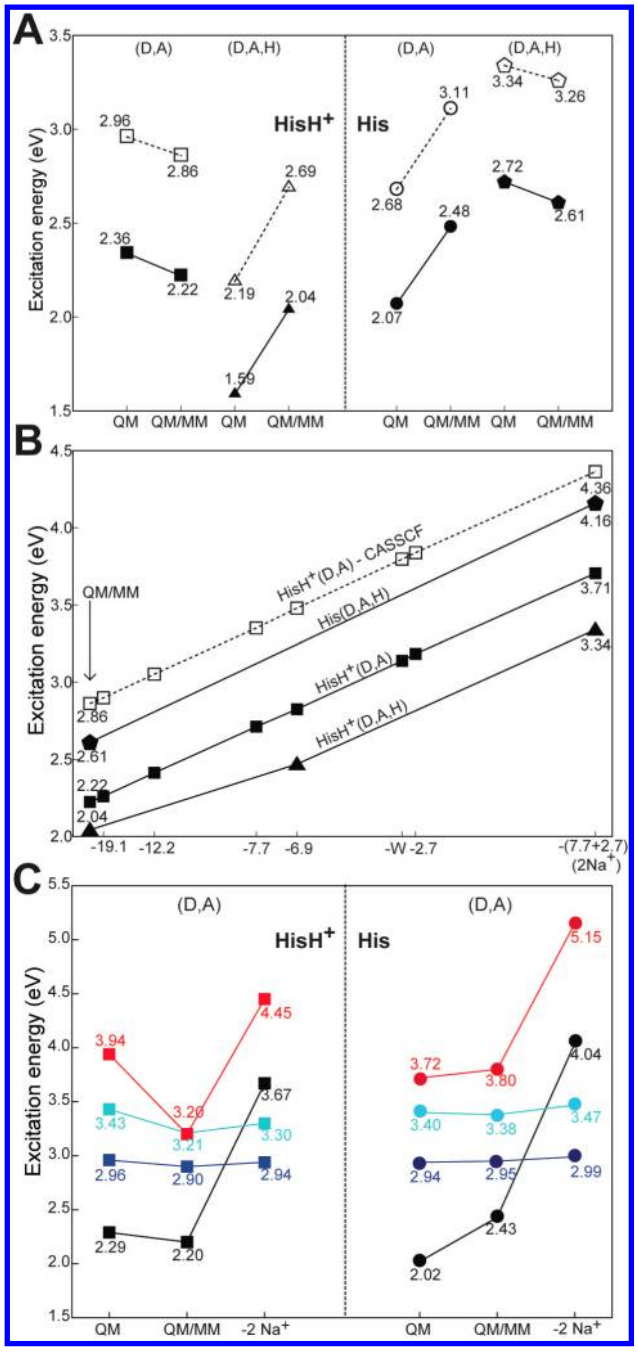

Figure 3. Excitation energies of the active site. (**A**) The ET-3′T excitation energy computed with the CASSCF(2,2)2-(MS)CASPT2 method. (**B**) The ET-3′T excitation energy computed with the CASSCF(2,2)2-(MS)CASPT2 method and models in which the MM part was modified. The energies of the $HisH^+$(D,A,H) models with MM-6.9 and MM-(2.7 + 7.7) were computed with the CASSCF-(2,3)3-(MS)CASPT2 method (see text). (**C**) The excitation energies computed with the CASSCF(2,5)5-(MS)CASPT2 method. The computed electronic states are ET-3′T (black), ET-5′T (red), LE1 (dark-blue), and LE2 (light-blue). In **A**–**C**, the models used for calculations are $HisH^+$(D,A) (squares), $HisH^+$(D,A,H) (triangles), His(D,A) (circles), and His(D,A,H) (pentagons). Filled symbols and solid lines indicate the (MS)CASPT2 energies; open symbols and dashed lines indicate the CASSCF energies.

The protonated histidine side chain included in the QM part is an electron acceptor that yields a low-lying ET state. This excited state becomes lower in energy than the ET-3′T state in the modified models MM-6.9 and MM-2Na^+. In these two models, the ET-$HisH^+$ excitation energy (not shown in Figure 3B) is 1.66 and 2.03 eV, whereas the ET-3′T energy (shown in Figure 3B) is 2.47 and 3.34 eV. These energies were computed with the CASSCF(2,3)3-(MS)CASPT2 method; the three-state ET-3′T energy is compared to the two-state energy of the unmodified model in Figure 3B. Notably, the same change of the environment increases the ET-$HisH^+$ energy by 0.37 eV, whereas the ET-3′T energy by 0.97 eV. Hence, not surprisingly, the electron-acceptor property of $His365H^+$ is influenced by the DNA charge to a lesser extent than that of the 3′ base.

For further characterization of the DNA repair site, we need to consider other excited states such as the LE states of the flavin chromophore and the ET states of other electron acceptors, in particular of the 5′ base. The LE states give rise to the flavin absorption and fluorescence spectrum. In contrast, the ET states are the "dark" states with no intensity in the absorption spectrum. In the photolyase, the electron transfer to the DNA substrate is primarily responsible for fluorescence quenching:[6] the flavin fluorescence lifetime is significantly reduced if the enzyme binds the photodamaged DNA. Because the calculations of the five electronic states are significantly more demanding, we considered only the smaller (D,A) models. The excitation energies are presented in Figure 3C. We note that the energies of the ET-3′T state obtained with the CASSCF(2,2)2-(MS)CASPT2 and CASSCF(2,5)5-(MS)-CASPT2 methods are very similar.

The two LE states of flavin correspond to the HOMO−LUMO and HOMO−(LUMO+1) $\pi\pi^*$ transitions with the energies around 2.95 eV (420 nm) and 3.40 eV (365 nm), respectively. The oscillator strengths of these transitions are 0.02 and 0.52, respectively, indicating that the lowest-energy LE1 state results in a weak absorption whereas the second LE2 state produces a strong band. This computational finding is in good agreement with the UV−vis spectrum of $FADH^-$ in photolyases[6,34] that have a strong band with a maximum around 380 nm and a low-intensity shoulder at the longer wavelengths. In photolyases, the weak LE1 transition is activated via energy transfer from the folate or deazaflavin antenna chromophore. Comparing the spectra computed for the protonated and neutral active sites, we find that the excitation energy of the LE1 state hardly changes. At the same time, the energy of the LE2 state decreases by 0.17 eV if the histidine is protonated. Our previous calculations based on supermolecular cluster models revealed a very similar trend—a decrease from 3.36 to 3.27 eV of the LE2 excitation energy and a slight increase from 2.59 to 2.63 eV of the LE1 energy upon histidine protonation.[11] (The cluster-model calculations in ref 11 were performed at the B3LYP-optimized geometry using the XMCQDPT2 method to compute the excitation energies.) Upon removing the Na^+ counterions, the LE1 and LE2 excitation energies practically stay unchanged.

Now we compare the ET states associated with the two bases of the (6−4) photoproduct. The oscillator strengths of the ET states are virtually zero, consistent with the role of these states in fluorescence quenching. The energy of the ET-5′T state is higher than that of the ET-3′T state. Protonation of histidine decreases both excitation energies: by 0.23 eV, the energy of the ET-3′T state (similar to what we found with the CASSCF(2,2)2 calculations of the (D,A) models), and by 0.59 eV, the energy of the ET-5′T state. A significantly larger effect on the ET-5′T-state energy is explained by the hydrogen bond that the 5′ base forms with His365. Upon removing the

dx.doi.org/10.1021/ct400537b | J. Chem. Theory Comput. 2013, 9, 4644−4652

two Na^+ ions, both excitation energies increase significantly: the 5′ base by 1.25 eV independent of the histidine protonation state and the 3′ base by 1.5 and 1.6 eV in the $HisH^+$ and His models, respectively. Similar to the two-state calculations, we find that the energy shifts due to the protonation and reduced screening of the DNA charge are practically independent of each other.

QM/MM Interaction Energies. The interaction energies of the QM part with the MM part in all considered electronic states are compared in Figure 4. The differences in the interaction energies of the ground and excited electronic states explain the differences in excitation energies computed with the QM/MM models as compared to the free QM part: If the ground state interacts stronger with the MM environment, the excitation energy increases; if the excited state interacts stronger, the excitation energy decreases. In our QM/MM models, the differences in the interaction energies have two contributions: the changes in the charge distribution and the polarization of the electronic states. The polarization of the environment is not considered in our model. As Figure 4 demonstrates, the interaction energy is essentially the ESPF energy, i.e., the interaction energy of the electrostatic charges. The differences in the ESPF energy also determine the trends in the excitation energies caused by the effect of the environment. The difference between the ESPF energy and the QM/MM interaction energy corresponds to the polarization energy of the QM part by the electrostatic charges of the MM part. The ESPF energies are always larger than the QM/MM interaction energies; thus the wave function polarization decreases the interaction energies of the active site with its environment. Despite the differences in the CASSCF- and CASPT2-computed electrostatic charges, the CASSCF- and CASPT2-computed ESPF energies are very similar in magnitude (data not shown). The smaller QM/MM interaction energies computed with the (MS)CASPT2 method compared to the CASSCF method demonstrate the increased wave function polarization in the former case. In the models with the modified MM-part, the increase of the ET excitation energies is explained by the decreasing interaction energies of the ET states. An exception is the $HisH^+$(D,A,H) model with the reversed trend: the ground state interacts stronger with the environment than the excited ET state; the interaction of the ground state is even further enhanced when the two Na^+ ions are removed. Obviously, this trend originates from the interactions of the cationic $HisH^+$ side chain with the electrostatic environment.

The analysis of the electrostatic charge distribution in the active site explains the differences in the interaction energies. Naturally, the most pronounced difference is found for the ET states in comparison with the ground state as demonstrated in Figure 5. Upon electron transfer, the electron acceptor gains a negative charge, whereas the isoalloxazine ring of the flavin semiquinone radical is neutral. We note a significant charge transfer from the 3′ base to the 5′ base in the ground and excited states.

Dynamic Electron Correlation. The comparison of dynamic electron-correlation energies of the considered electronic states computed as a difference of the (MS)CASPT2 and CASSCF excitation energies is presented in Figure 6. The differential dynamic electron-correlation energy has a tendency to increase with the increase of the excitation energy. Interestingly, the two-state calculations for the ET 3′T state are characterized by a smaller dynamic-correlation energy correction than the respective five-state calculations. This difference is explained by the differences in the respective CASSCF excitation energies: the ET-3′T excitation energy computed with the CASSCF(2,2)2 method is smaller than that computed with CASSCF(2,5)5, but after the (MS)CASPT2 correction very similar excitation energies are obtained with both methods. In Figure 6, two trends can be distinguished: one for the ET states and the other for the LE states.

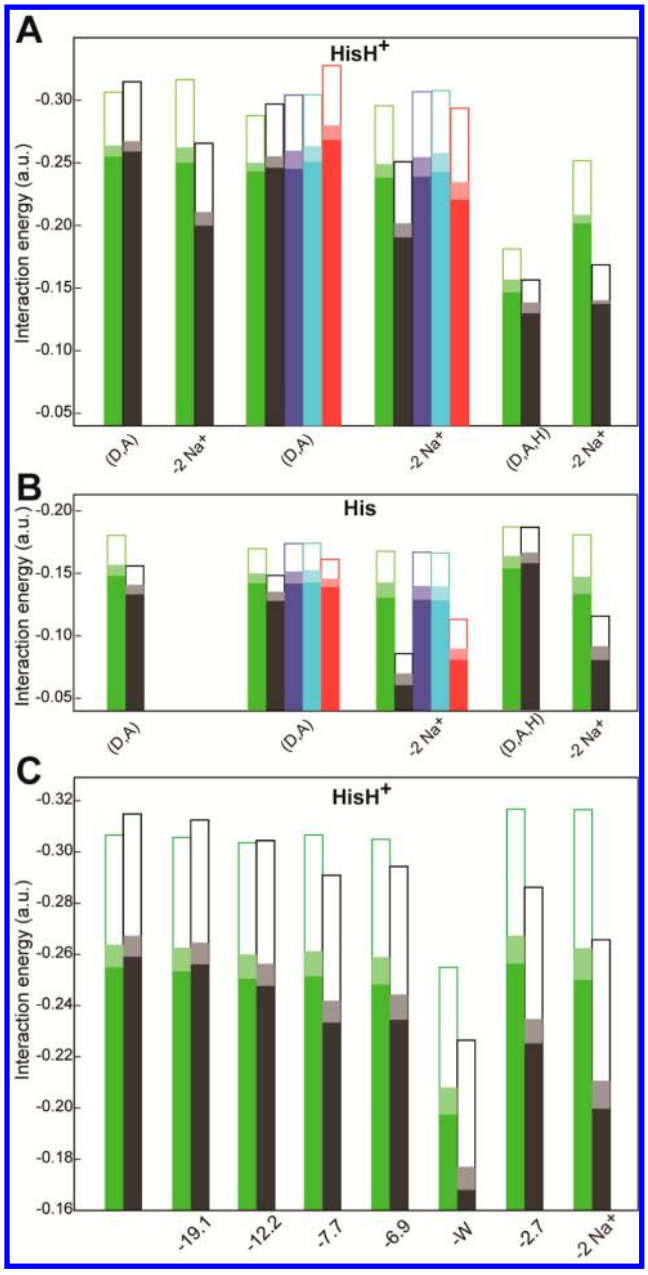

Figure 4. The QM/MM interaction energies of the $HisH^+$ models (**A**), His models (**B**), and $HisH^+$ models with the modified MM part (**C**). The electronic states are the closed-shell ground state (green), ET-3′T (black), ET-5′T (red), LE1 (dark-blue), and LE2 (light-blue). Open bars indicate the ESPF interaction energies computed with the CASSCF method. Light-colored filled bars indicate the CASSCF QM/MM interaction energies. Dark-colored filled bars indicate the (MS)CASPT2 QM/MM interaction energies. The two- and five-bar diagrams represent the CASSCF(2,2)2-(MS)CASPT2 and CASSCF-(2,5)5-(MS)CASPT2 calculations, respectively.

dx.doi.org/10.1021/ct400537b | J. Chem. Theory Comput. 2013, 9, 4644−4652

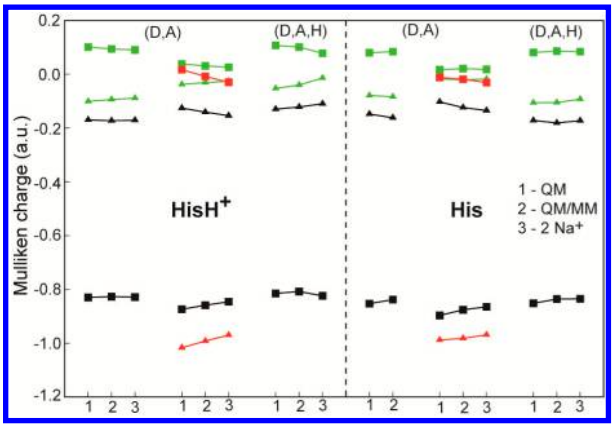

Figure 5. Mulliken electrostatic charges of the 3′ base (triangles) and the 5′ base (squares) in the ground closed-shell (green), ET-3′T (black), and ET-5′T (red) electronic states computed with the CASSCF method. The two-color diagrams are computed with CASSCF(2,2)2; the three-color diagrams are computed with the CASSCF(2,5)5 method.

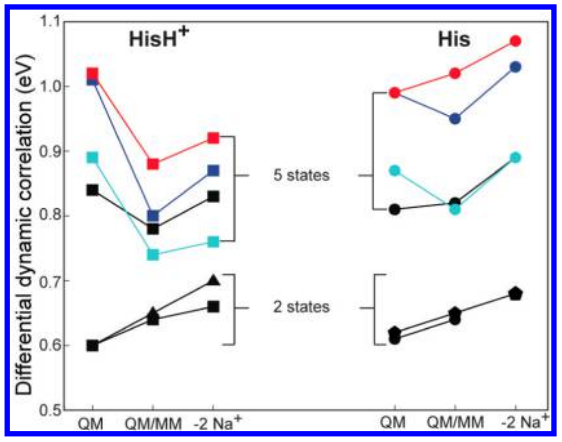

Figure 6. Differential dynamic electron-correlation energy computed as a difference between the (MS)CASPT2 and CASSCF excitation energies. The electronic states are ET-3′T (black), ET-5′T (red), LE1 (dark-blue), and LE2 (light-blue). The models used for calculations are HisH$^+$(D,A) (squares), HisH$^+$(D,A,H) (triangles), His(D,A) (circles), and His(D,A,H) (pentagons). "5-state" and "2-state" indicate the CASSCF(2,5)5-(MS)CASPT2 and CASSCF(2,2)2-(MS)CASPT2 calculations, respectively.

DISCUSSION AND CONCLUSIONS

We computed excitation energies of the DNA repair active site in the (6−4) photolyase−DNA macromolecular complex employing the hybrid QM/MM approach with the goal to study the effects of the environment on photoinduced electron transfer implicated in DNA repair. In particular, we computed the energies of the two LE states of the anionic flavin hydroquinone and the ET states of three electron acceptors: the two nucleobases of the photoproduct and the protonated histidine His365H$^+$. These acceptors contribute to the quenching of flavin fluorescence in the photolyase−DNA complex. To compute on equal footing the LE and ET states, we include the electron donor and the electron acceptor in the QM part. Two types of the environmental effects are of our interest: (i) protonation of the histidine in the enzymatic active site, which we evaluate by comparing the "protonated" and "neutral" active site models, and (ii) the effect of the DNA negative charge, which we probed by altering the coordinates of the Na$^+$ counterions in the MM part. We also analyzed how variations in the quantum-mechanical description such as including the dynamic electron correlation and considering different numbers of electronic states influence the excitation energies. The dynamic electron-correlation correction decreases the excitation energies with differential effects. Nevertheless, the effects of the environment on the excitation energy have a similar magnitude with the CASSCF and CASPT2 methods.

The vertical excitation energies of the LE states are in good agreement with the excitation spectrum of the reduced flavin in the photolyase enzyme[6,34] and also with the energies previously computed by us with the supermolecular cluster models.[11] Comparison of the cluster models and the QM/MM models is presented in Figure 7A. Among all considered states, the LE1

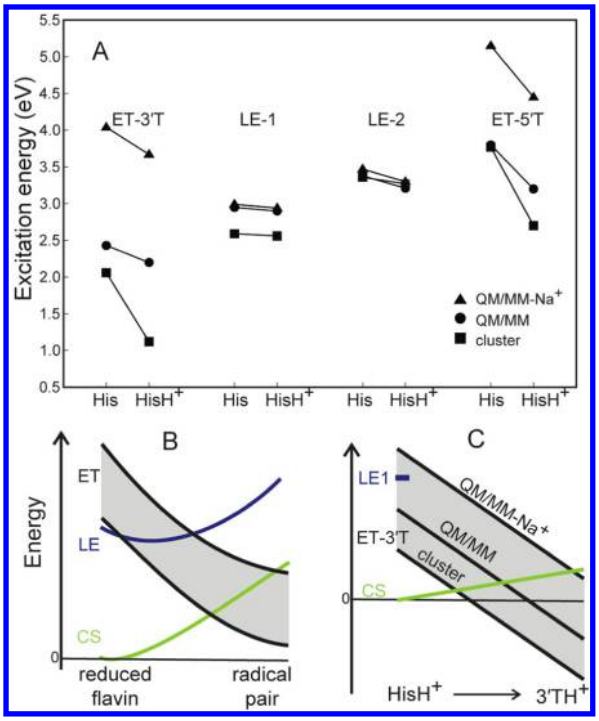

Figure 7. Electron and proton transfer energies. (**A**) Comparison of the excitation energies obtained with the QM/MM models and cluster models.[11] (**B**) The change of the ET-state energy along the electron-transfer pathway leads to changes in the lifetimes of the excited flavin and radical pair. The higher ET energies result from the decreased screening of the DNA negative charge; the lower ET energies result from the protonation of the active site, screening (or omitting) of the DNA charge, and also extending the QM part. (**C**) Energies along the proton-coupled electron transfer reaction coordinate. Electron transfer from FADH$^-$ to 3′ base, proton transfer from His365H$^+$ to 3′ base, and the QM/MM energies of the protonated 3′ base model are determined by energy extrapolation on the basis of the cluster-model results.[11]

state of flavin is least affected by interactions with the ionic groups. The excitation energy of the LE2 state slightly decreases from 3.4 to 3.2 eV upon histidine protonation. The DNA negative charge has a negligible effect on the LE excitation energies. In contrast, the excitation energies of the ET states are very sensitive to the presence of ionic groups. Protonation of the histidine leads to a significant stabilization of the ET states, especially in the models including histidine in the

dx.doi.org/10.1021/ct400537b | J. Chem. Theory Comput. 2013, 9, 4644−4652

QM part. The DNA negative charge has an opposite effect, significantly increasing the ET excitation energies.

We note that the cluster models predict smaller ET excitation energies than the QM/MM models. Lowering the ET-3′T energy is also observed upon extending the QM part by including the histidine side chain. This finding indicates that intermolecular interactions other than the electrostatic interactions, i.e., mutual polarization of the chromophore and environment, charge-transfer, and dispersion that are not included in the QM/MM model, contribute to stabilization of the ET states. To account for these effects, we need to extend the QM part in the QM/MM models, which is currently prohibitive due to the high computational cost. Another way of improving the QM/MM description is including the polarization of the environment (recently reviewed in ref 35). Accounting for the environment polarization may compensate the electrostatic-induced excitation-energy shifts as it is demonstrated for the tryptophan chromophore embedded in the human serum albumin protein.[35] Our cluster and QM/MM models predict energies of the ET states to be within a rather large energy interval—the lower bound is provided by our cluster models, and the upper bound is provided by our QM/MM-Na^+ model as shown in Figure 7A. We note that the differences in the ET excitation energies due to the variations of the molecular models are very large. Obviously, neither cluster nor QM/MM models represent an optimal choice. In fact, the choice of the model rather than the choice of the QM method may determine the accuracy of computations. Finding a balance between these two computational aspects represents, in our opinion, the major challenge faced in quantum-mechanical computations of the electron-transfer energies.

The dependence of the photoproduct's ET energies on the screening of the DNA negative charge points toward a potential drastic difference in the intrinsic properties of the nucleobases and the properties of DNA. To the best of our knowledge, the exciting picture of the DNA properties does not back up such a conjecture in general. In the context of the DNA-repair calculations, this finding indicates that the QM/MM models may predict varying fluorescence lifetimes, electron-transfer rates, and radical-recombination rates depending on how the DNA substrate is treated. As depicted in Figure 7B, models with the less-screened DNA, for instance, the one employed in the study of ref 14, should predict a longer flavin fluorescence lifetime and higher-energy radical pairs which undergo recombination more readily, whereas models with the more-screened DNA should predict shorter-lived fluorescence and more stable radical pairs. An important factor in DNA screening is the solvating water-shell, which is not present in the crystal structure but should be introduced in the QM/MM model. To obtain more reliable ET energy estimates we should study the counterion distribution with the classical molecular dynamics and identify the putative binding sites close to the active site (within about 12 Å from the phosphorus atom) in the photolyase−DNA complex.

We extended the QM part by including the histidine side chain in order to compute protonation of the (6−4) photoproduct by the histidine in our further studies. This protonation, following photoinduced electron transfer, is considered by several authors to be a critical step in the DNA repair mechanism.[12,14,15] The resulting electron and proton transfer model is computationally very demanding to use for the QM/MM geometry optimization with the CASSCF method or for computing the higher-energy excited states. Nevertheless, we were able to compare the excitation energy of the flavin-photoproduct ET-3′T state computed with the models containing the neutral or protonated His365 side chain in the QM part. In Figure 7C, we show, according to our previous calculations,[11] that proton and electron transfer lowers the energy of the ET-3′T state, which becomes the ground state. The excited-state energy decrease upon proton transfer is 2.7 eV. This decrease significantly exceeds the increase of the ET-3′T-state excitation energy in the QM/MM-Na^+ models, in which electron transfer is hindered. Therefore, we can expect the ground-state proton coupled electron transfer to take place even under the unfavorable conditions of the reduced DNA screening. This preliminary result suggests that the deactivation of the enzyme via the ground-state proton-coupled electron transfer is a likely process. In experiments, this enzyme's deactivation is probably observed upon lowering the pH from 9 to 7.[4] Thus, the proposed catalytic role of protonation must be carefully re-evaluated not only by further computational studies but also by specifically designed experiments. We also found that protonated His365H^+ is a plausible electron acceptor, which may contribute to the quenching of the $FADH^-$ fluorescence at the proton concentration lower than the pK_a of His365.

For the wild-type (6−4) photolyase and a series of its His365 mutants, electron transfer dynamics have been characterized by means of ultrafast spectroscopy.[6] In these proteins without the DNA−substrate bound, the lifetime of flavin fluorescence ranges from 4 to 1.7 ns. Upon DNA−substrate binding, the fluorescence lifetime decreases at least by an order of magnitude, revealing that the ET states of the photoproduct are involved in fluorescence quenching. Our calculations presented here reveal that the ET-3′T and ET-5′T states are the electronic states contributing to the quenching process. Only in the wild-type protein (containing His365) does the electron-transfer process with the time constant of 225 ps result in DNA repair. In the mutated proteins, the time constants vary from 281 to 147 ps, but no repair takes place. In the original paper,[6] this observation was interpreted as evidence for the presence of the protonated His365H^+ side chain. However, there is no correlation between the determined electron-transfer rates and the electrostatic charge or polarity of the mutated side chain. This observation rather agrees with the notion supported by our studies that the repair-competent active site contains the neutral His365 side chain. Interestingly, in the photodynamic experiments, protonated cationic lysine is similar to deprotonated anionic aspartate and neutral alanine (time constants 281, 278, and 274 ps, respectively),[6] indicating that the presence of the charged side chain is unlikely to play a role in the observed rates. The wild-type photolyase is similar to the mutants with neutral residues methionine and tyrosine (time constants 225, 232, and 249 ps, respectively).[6] The most short-lived fluorescence (time constant 147 ps) was found in the asparagine mutant.[6] These intriguing observations await an explanation. For the development of adequate kinetic models, computational models that evaluate electron-transfer rates quantum-mechanically and also combine the account of various relevant effects, for instance protein and DNA molecular dynamics, are indispensible despite all technical challenges and complexity. Our work constitutes the first step toward this goal.

■ ASSOCIATED CONTENT

Supporting Information

Selected distances in the optimized geometries are compared in Figure S1. All computed energies are collected in Tables S1 and S2, the Mulliken charges in Tables S3 and S4, and the Cartesian coordinates of the optimized geometries of the QM parts in Tables S5 and S6. This information is available free of charge via the Internet at http://pubs.acs.org.

■ AUTHOR INFORMATION

Corresponding Author

*E-mail: Tatjana.Domratcheva@mpimf-heidelberg.mpg.de.

Notes

The authors declare no competing financial interest.

■ ACKNOWLEDGMENTS

We are very grateful to Chris Roome for the excellent assistance in high-performance computing, to Nicolas Ferré (Aix Marseille Université) for computational advice, and to Ilme Schlichting for collaboration and support. We acknowledge financial support from the MPG Minerva program (T.D.) and BIOMS-Heidelberg (A.R.M.S.).

■ REFERENCES

(1) Weber, S. *Biochim. Biophys. Acta* **2005**, *1707*, 1−23.
(2) Sancar, A. *J. Biol. Chem.* **2008**, *283*, 32153−32157.
(3) Muller, M.; Carell, T. *Curr. Opin. Struct. Biol.* **2009**, *19*, 277−285.
(4) Hitomi, K.; Nakamura, H.; Kim, S. T.; Mizukoshi, T.; Ishikawa, T.; Iwai, S.; Todo, T. *J. Biol. Chem.* **2001**, *276*, 10103−10109.
(5) Schleicher, E.; Hitomi, K.; Kay, C. W.; Getzoff, E. D.; Todo, T.; Weber, S. *J. Biol. Chem.* **2007**, *282*, 4738−4747.
(6) Li, J.; Liu, Z. Y.; Tan, C.; Guo, X. M.; Wang, L. J.; Sancar, A.; Zhong, D. P. *Nature* **2010**, *466*, 887−890.
(7) Maul, M. J.; Barends, T. R. M.; Glas, A. F.; Cryle, M. J.; Domratcheva, T.; Schneider, S.; Schlichting, I.; Carell, T. *Angew. Chem., Int. Ed.* **2008**, *47*, 10076−10080.
(8) Fingerhut, B. P.; Heil, K.; Kaya, E.; Oesterling, S.; de Vivie-Riedle, R.; Carell, T. *Chem. Sci.* **2012**, *3*, 1794−1797.
(9) Domratcheva, T.; Schlichting, I. *J. Am. Chem. Soc.* **2009**, *131*, 17793−17799.
(10) Harbach, P. H. P.; Borowka, J.; Bohnwagner, M. V.; Dreuw, A. *J. Phys. Chem. Lett.* **2010**, *1*, 2556−2560.
(11) Domratcheva, T. *J. Am. Chem. Soc.* **2011**, *133*, 18172−18182.
(12) Faraji, S.; Dreuw, A. *J. Phys. Chem. Lett.* **2012**, *3*, 227−230.
(13) Condic-Jurkic, K.; Smith, A. S.; Zipse, H.; Smith, D. M. *J. Chem. Theory Comput.* **2012**, *8*, 1078−1091.
(14) Sadeghian, K.; Bocola, M.; Merz, T.; Schutz, M. *J. Am. Chem. Soc.* **2010**, *132*, 16285−16295.
(15) Ai, Y. J.; Liao, R. Z.; Chen, S. L.; Hua, W. J.; Fang, W. H.; Luo, Y. *J. Phys. Chem. B* **2011**, *115*, 10976−10982.
(16) Ferre, N.; Angyan, J. G. *Chem. Phys. Lett.* **2002**, *356*, 331−339.
(17) Aquilante, F.; De Vico, L.; Ferre, N.; Ghigo, G.; Malmqvist, P. A.; Neograd y, P.; Pedersen, T. B.; Pitonak, M.; Reiher, M.; Roos, B. O.; Serrano-Andres, L.; Urban, M.; Veryazov, V.; Lindh, R. *J. Comput. Chem.* **2010**, *31*, 224−247.
(18) Karlstrom, G.; Lindh, R.; Malmqvist, P. A.; Roos, B. O.; Ryde, U.; Veryazov, V.; Widmark, P. O.; Cossi, M.; Schimmelpfennig, B.; Neograd y, P.; Seijo, L. *Comput. Mater. Sci.* **2003**, *28*, 222−239.
(19) Ponder, J. W. TINKER: Software tools for molecular design, version 5.1. http://dasher.wustl.edu/tinker (Accessed: August 2013).
(20) Roos, B. O.; Andersson, K.; Fulscher, M. P.; Malmqvist, P. A.; Serrano Andres, L.; Pierloot, K.; Merchan, M. *Adv. Chem. Phys.* **1996**, *93*, 219−331.
(21) Andersson, K.; Malmqvist, P. A.; Roos, B. O. *J. Chem. Phys.* **1992**, *96*, 1218−1226.
(22) Finley, J.; Malmqvist, P. A.; Roos, B. O.; Serrano-Andres, L. *Chem. Phys. Lett.* **1998**, *288*, 299−306.
(23) Harihara, P.; Pople, J. A. *Theor. Chim. Acta* **1973**, *28*, 213−222.
(24) Cornell, W. D.; Cieplak, P.; Bayly, C. I.; Gould, I. R.; Merz, K. M.; Ferguson, D. M.; Spellmeyer, D. C.; Fox, T.; Caldwell, J. W.; Kollman, P. A. *J. Am. Chem. Soc.* **1996**, *118*, 2309−2309.
(25) Jorgensen, W. L.; Chandrasekhar, J.; Madura, J. D.; Impey, R. W.; Klein, M. L. *J. Chem. Phys.* **1983**, *79*, 926−935.
(26) Martinez, L.; Andrade, R.; Birgin, E. G.; Martinez, J. M. *J. Comput. Chem.* **2009**, *30*, 2157−2164.
(27) Masson, F.; Laino, T.; Rothlisberger, U.; Hutter, J. *Chem. Phys. Chem.* **2009**, *10*, 400−410.
(28) Spector, T. I.; Cheatham, T. E.; Kollman, P. A. *J. Am. Chem. Soc.* **1997**, *119*, 7095−7104.
(29) Humbel, S.; Sieber, S.; Morokuma, K. *J. Chem. Phys.* **1996**, *105*, 1959−1967.
(30) Sherwood, P.; de Vries, A. H.; Collins, S. J.; Greatbanks, S. P.; Burton, N. A.; Vincent, M. A.; Hillier, I. H. *Faraday Discuss.* **1997**, *106*, 79−92.
(31) Melaccio, F.; Olivucci, M.; Lindh, R.; Ferre, N. *Int. J. Quantum Chem.* **2011**, *111*, 3339−3346.
(32) Ghigo, G.; Roos, B. O.; Malmqvist, P. A. *Chem. Phys. Lett.* **2004**, *396*, 142−149.
(33) Forsberg, N.; Malmqvist, P. A. *Chem. Phys. Lett.* **1997**, *274*, 196−204.
(34) Kao, Y. T.; Saxena, C.; Wang, L. J.; Sancar, A.; Zhong, D. P. *Proc. Natl. Acad. Sci. U. S. A.* **2005**, *102*, 16128−16132.
(35) Monari, A.; Rivail, J.-L.; Assfeld, X. *Acc. Chem. Res.* **2013**, *46*, 596−603.